Proc. of the 16th Int. Conference on Digital Audio Effects (DAFx-13), Maynooth, Ireland, September 2-5, 2013

FOURTH-ORDER AND OPTIMISED FINITE DIFFERENCE SCHEMES FOR THE 2-D WAVE EQUATION

Brian Hamilton, *

Acoustics and Audio Group
University of Edinburgh
b.hamilton-2@sms.ed.ac.uk

Stefan Bilbao,

Acoustics and Audio Group
University of Edinburgh
sbilbao@staffmail.ed.ac.uk

ABSTRACT

This paper investigates some fourth-order accurate explicit finite difference schemes for the 2-D wave equation obtained using 13-, 17-, 21-, and 25-point discrete Laplacians. Optimisation is conducted in order to minimise numerical dispersion and computational costs. New schemes are presented that are more computationally efficient than nine-point explicit schemes at maintaining less than one percent wave speed error up to some critical frequency. Simulation results are presented.

1. INTRODUCTION

Finite difference (FD) schemes for the 2-D wave equation [1] have long been used for seismic simulations [2], sound synthesis based on physical models of membranes [3], and as a starting point for modelling 3-D room acoustics [4]. Numerical dispersion in FD approximations can cause audible artifacts such as a mistuning of modes [5] and smearing of transients by a non-linear phase/group delay [6]. Minimising this error in a computationally efficient manner is one of the main concerns in using FD methods for audio and acoustical applications [5].

There are generally two approaches to minimising the effect of numerical dispersion up to some audible frequency of interest. The first strategy is to choose a simple FD scheme and reduce the grid spacing (oversample the grid) until the continuous frequency of interest maps to some discrete frequency whose wave speed error is negligible. However, as the grid spacing is reduced in N-dimensional space computational costs scale to the (N+1)th power and memory usage scales to the Nth power, so this strategy has limited use in practice. For example, the computation of large-scale 3-D room acoustics can be accelerated through the use of graphics processing units (GPUs) [7, 8], but reducing the grid spacing quickly shrinks the available room volume due to finite memory on the GPU cards.

When the practical limit of this strategy is reached, another must be pursued, which is to improve the FD approximation by employing more points from the grid [6, 9–14]. This leads to another set of issues, such as optimising any free parameters, finding stability conditions, and terminating the spatial domain with suitable boundary conditions. The FD schemes that have seen wide use in the context of musical and room acoustics have been second-order accurate. Fourth-order accurate (in space and time) FD schemes result in less numerical dispersion at low frequencies than second-order schemes [9, 12, 13, 15] and typically this reduces the dispersion in higher frequencies to some extent. Fourth-order schemes can be achieved using nine-point implicit formulations on the square grid [12, 16], but implicit schemes are less parallelisable than explicit schemes, so they are less attractive for GPU implementations. Explicit fourth-order accurate schemes can be achieved by employing more than nine points on the square grid [9, 15]. Such schemes increase the difficulty in terminating the grid, but boundary conditions beyond the fixed type (used for membranes [17]) will be left out of this study.

This study focuses on a family of fourth-order accurate explicit 2-D schemes employing 13, 17, 21, or 25 spatial points [9, 15]. Many of these schemes have already been identified [9], but certain special cases have not been investigated in previous studies [9, 15]. The interest here is to reduce numerical dispersion over the range of audible frequencies, so optimisation will be conducted in order to trade traditional accuracy (order of accuracy) for a spectral-like accuracy [18]. This should lead to more perceptually accurate results, but perceptual tests are out of the scope of this study. In contrast to [15], the optimisation conducted here will take into account a measure of computational costs [13].

The paper is structured as follows: in Section 2, the parameterised 25-point FD scheme is presented along with stability conditions, numerical dispersion, and computational density. In Section 3, conditions for fourth-order accuracy are derived and some optimal fourth-order accurate schemes are presented. In Section 4, results of optimisation are presented and conclusions are given in Section 5.

2. BACKGROUND

2.1. 2-D Wave Equation

Using the abbreviation $\partial_w^p = \frac{\partial^p}{\partial w^p}$ for some variable $w \in \mathbb{R}$ and $p \in \mathbb{N}^+$ (positive integers) , the 2-D wave equation can be written as:

$$\Box u = 0\,, \quad \Box = \partial_t^2 - c^2\Delta\,, \quad \Delta = \partial_x^2 + \partial_y^2\,, \qquad (1)$$

where $\Box$ is the d'Alembert operator (d'Alembertian), c is the wave speed, Δ is the 2-D Laplace operator (Laplacian), t is time, and $u = u(t, \boldsymbol{x})$ is the solution to be approximated for $\boldsymbol{x} \in \mathbb{R}^2$, $\boldsymbol{x} = (x, y)$. For acoustics, the variable u can represent pressure, a velocity potential, or the displacement of a membrane [19].

2.2. Time Difference Operators

The standard three-step approximation to ∂_t^2 in explicit FD schemes for the wave equation is the FD operator δ_{tt}:

$$\delta_{tt}\hat{u} = \frac{1}{k^2}\left(\hat{u}(t+k, \boldsymbol{x}) - 2\hat{u}(t, \boldsymbol{x}) + \hat{u}(t-k, \boldsymbol{x})\right)\,, \qquad (2)$$

* This work was supported by the European Research Council, under grant StG-2011-279068-NESS, and by the Natural Sciences and Engineering Research Council of Canada.

where k is the time-step, which can be set to $1/F_s$, where F_s is an audio sampling rate like 44.1 kHz. The variable $\hat{u} = \hat{u}(t, \boldsymbol{x})$ represents the FD approximation to $u(t, \boldsymbol{x})$.

2.3. Finite difference approximations to the Laplacian

Let $\Omega \subset \mathbb{R}^2$ be a finite set of equal-norm vectors and let $|\Omega|$ denote its cardinality. Approximations to the Laplacian can be built using the FD operator:

$$\delta_{\Delta,\Omega}\hat{u} = \frac{\kappa}{h^2}\sum_{i=1}^{|\Omega|}(\hat{u}(t,\boldsymbol{x}+\boldsymbol{v}_i h)-2\hat{u}(t,\boldsymbol{x})+\hat{u}(t,\boldsymbol{x}-\boldsymbol{v}_i h))\,, \quad (3)$$

where h is the spatial step, $\boldsymbol{v}_i \in \Omega$, and κ will be chosen according to consistency conditions. This will be called a $(2|\Omega|+1)$-point *discrete Laplacian* or *stencil*. The following sets of vectors coming from the first five shells of points on the $\mathbb{Z}^2$ lattice, as seen in Fig. 1, will be investigated:

$$\begin{aligned} &\Omega_1 = \{\hat{\boldsymbol{e}}_x, \hat{\boldsymbol{e}}_y\}, \quad \Omega_2 = \{\hat{\boldsymbol{e}}_x + \hat{\boldsymbol{e}}_y, \hat{\boldsymbol{e}}_x - \hat{\boldsymbol{e}}_y\}, \quad (4)\\ &\Omega_3 = 2\Omega_1, \qquad \Omega_4 = \{2\hat{\boldsymbol{e}}_x \pm \hat{\boldsymbol{e}}_y, \hat{\boldsymbol{e}}_x \pm 2\hat{\boldsymbol{e}}_y\}, \quad \Omega_5 = 2\Omega_2\,. \end{aligned}$$

For these choices of Ω the condition on κ for consistency is:

$$\kappa = \frac{2}{|\Omega|\|\boldsymbol{v}\|^2}\,, \quad (5)$$

where $\|\boldsymbol{v}\|$ denotes the Euclidean norm of any $\boldsymbol{v} \in \Omega$.

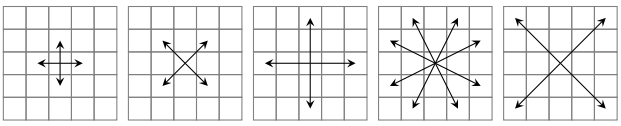

(a) $j = 1$ (b) $j = 2$ (c) $j = 3$ (d) $j = 4$ (e) $j = 5$

Figure 1: *Vectors in* $-\Omega_j \cup \Omega_j$.

An approximation to the Laplacian can also be built as a linear combination of these stencils:

$$\delta_{\boldsymbol{\Delta},\boldsymbol{\alpha},\Upsilon}\hat{u} = \sum_{j=1}^{5}\alpha_j\delta_{\Delta,\Omega_j}\hat{u}\,, \quad (6)$$

where $\Upsilon = \{\Omega_1, \Omega_2, \Omega_3, \Omega_4, \Omega_5\}$ is a *set of sets* and $\boldsymbol{\alpha} \in \mathbb{R}^5$. The following condition on $\boldsymbol{\alpha}$ is required for consistency:

$$\sum_{j=1}^{5}\alpha_j = 1\,. \quad (7)$$

The discrete Laplacian $\delta_{\boldsymbol{\Delta},\boldsymbol{\alpha},\Upsilon}$ employs either 5, 9, 13, 17, 21, or 25 points depending on the number of non-zero elements in $\boldsymbol{\alpha}$.

2.4. Finite Difference Scheme for the 2-D Wave Equation

Combining these operators gives a FD scheme for the 2-D wave equation:

$$\delta_{\Box}\hat{u} = 0\,, \quad \delta_{\Box} = \delta_{tt} - c^2\delta_{\boldsymbol{\Delta},\boldsymbol{\alpha},\Upsilon}\,, \quad (8)$$

where $\delta_{\Box}$ is the *discrete d'Alembertian*. The approximation is updated in time with the explicit recursion:

$$\hat{u}(t+k,\boldsymbol{x}) = (c^2k^2\delta_{\boldsymbol{\Delta},\boldsymbol{\alpha},\Upsilon} + 2)\hat{u}(t,\boldsymbol{x}) - \hat{u}(t-k,\boldsymbol{x}) \quad (9)$$

given some initial conditions. The FD scheme will only be calculated at a set of points in space and time pertaining to some grid. The grid for time will be the $\mathbb{Z}$ lattice, scaled by the time-step k, and the spatial lattice (grid) will be the $\mathbb{Z}^2$ lattice, scaled by the spatial step h.

2.5. Stability

Using von Neumann stability analysis [20] it is sufficient to consider a plane wave of the form $\hat{u}(t,\boldsymbol{x}) = e^{j(\omega t + \boldsymbol{\xi}\cdot\boldsymbol{x})}$, where ω is the temporal frequency, $\boldsymbol{\xi}$ is the *wave vector* of spatial frequencies, or *wavenumbers*, and $(\omega, \boldsymbol{\xi}) \in \mathbb{R}^3$. It is convenient to define a normalised wavenumber $\boldsymbol{\xi}_h = \boldsymbol{\xi}h$ and normalised frequency $\omega_k = \omega k$ [15]. Then, inserting the plane wave into (8) gives:

$$\frac{1}{k^2}\mathcal{D}_{tt}(\omega_k) - \frac{c^2}{h^2}\mathcal{D}_{\boldsymbol{\Delta},\boldsymbol{\alpha},\Upsilon}(\boldsymbol{\xi}_h) = 0\,, \quad (10)$$

where

$$\mathcal{D}_{tt}(\omega_k) = -4\sin^2(\omega_k/2)\,, \quad (11)$$

$$\mathcal{D}_{\boldsymbol{\Delta},\boldsymbol{\alpha},\Upsilon}(\boldsymbol{\xi}_h) = -4\sum_{j=1}^{5}\alpha_j\kappa_j\sum_{i=1}^{|\Omega_j|}\sin^2(\boldsymbol{\xi}_h\cdot\boldsymbol{v}_{j,i}/2)\,, \quad (12)$$

and where $\boldsymbol{v}_{j,i} \in \Omega_j$. The scheme is stable if no real wavenumbers produce growing solutions in time [20]. Along with a non-positivity constraint on $\mathcal{D}_{\boldsymbol{\Delta},\boldsymbol{\alpha},\Upsilon}$ that is generally satisfied, the condition for stability becomes:

$$\lambda \leq \lambda_{\max,\boldsymbol{\alpha}} = \sqrt{\frac{4}{\max_{\boldsymbol{\xi}_h}|\mathcal{D}_{\boldsymbol{\Delta},\boldsymbol{\alpha},\Upsilon}(\boldsymbol{\xi}_h)|}}\,, \quad (13)$$

where $\lambda = ck/h$ is the Courant number. In many of schemes that will be featured, $\lambda_{\max,\boldsymbol{\alpha}}$ can be found at $\boldsymbol{\xi}_h = (\pi, \pi)$ [9], but this is not true in general for the whole parameter space of $\boldsymbol{\alpha}$. Apart from simple cases, finding $\lambda_{\max,\boldsymbol{\alpha}}$ as a function of $\boldsymbol{\alpha} \in \mathbb{R}^5$ can become quite involved, but it can be found numerically to sufficient precision for practical applications when an analytic expression is out of reach.

2.6. Numerical Dispersion

Unless the FD scheme provides an *exact* approximation to the solution of the wave equation, which is only possible in 1-D [12], the numerical wave speed in the approximation $\hat{u}(t,\boldsymbol{x})$ becomes frequency- and direction-dependent. The *relative phase velocity* (this will also be referred to as the *numerical* or *relative wave speed*) is:

$$\hat{\nu}(\boldsymbol{\xi}_h) = \frac{\omega_k(\boldsymbol{\xi}_h)}{\lambda|\boldsymbol{\xi}_h|}\,, \quad \omega_k(\boldsymbol{\xi}_h) = \mathcal{D}_{tt}^{-1}(\lambda^2\mathcal{D}_{\boldsymbol{\Delta},\boldsymbol{\alpha},\Upsilon}(\boldsymbol{\xi}_h)) \quad (14)$$

for $\omega_k \in (0,\pi]$ and $\boldsymbol{\xi}_h \in (0,\pi]\times(0,\pi]$. In the ideal case, $\hat{\nu}(\boldsymbol{\xi}_h) = 1$, corresponding to a phase velocity of c.

Using the dispersion relation the wave speed error as a function of wavenumbers can be reassigned to temporal frequencies ω and angles of propagation θ [13]:

$$\hat{\nu}(\omega_k(|\boldsymbol{\xi}_h|,\theta),\theta) = \frac{\omega_k(|\boldsymbol{\xi}_h|,\theta)}{\lambda|\boldsymbol{\xi}_h|}\,, \quad (15)$$

where $\boldsymbol{\xi}_h$ is written in polar form $\boldsymbol{\xi}_h = (|\boldsymbol{\xi}_h|,\theta)$ and $\theta \in [0,\pi/2]$. This representation is useful for audio applications because it shows

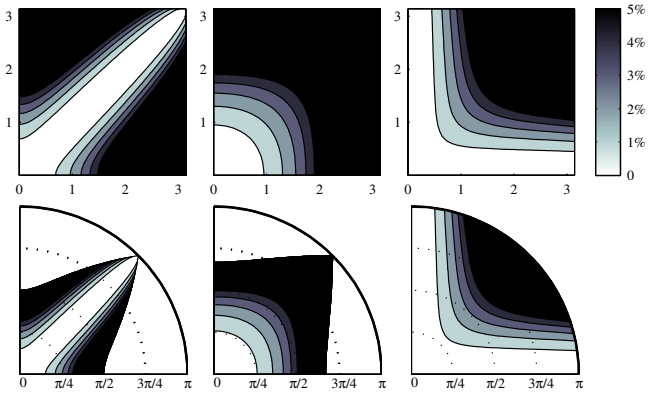

(a) *5-point* (b) *9-point, iso* (c) *9-point, IWB*

Figure 2: *Relative wave speed error* $(|1-\hat{\nu}|)$ *as a function of* $\boldsymbol{\xi}_h$ *(top row) and as a function of* ω_k *and* θ *(bottom row). Contours denote 1% deviations in the error. Any error beyond 5% is coloured in black.*

how the wave speed error maps to audible (temporal) frequencies, and it demonstrates direction-dependent cutoff frequencies [13]. The absolute wave speed errors of the standard five-point scheme [1] $(\lambda = \sqrt{1/2}, \boldsymbol{\alpha} = (1, \mathbf{0}))$ and the nine-point isotropic scheme [6] $(\lambda = \sqrt{3/4}, \boldsymbol{\alpha} = (1/3, 2/3, \mathbf{0}))$ and the *interpolated wideband* (IWB) scheme [13] $(\lambda = 1, \boldsymbol{\alpha} = (1/2, 1/2, \mathbf{0}))$ are plotted in Fig. 2 with 1% contours. Beyond 5% error will not be considered, so it is coloured black.

2.7. Computational Density

The *computational density* of a FD scheme is the number updates per unit time and space. On the square grid this is $(h^2 k)^{-1}$. Fixing λ and c the computational density can be written as $(c/\lambda)h^{-3}$. The computational density of each scheme can then be normalised by choosing the spatial step to be $h = \sqrt[3]{1/\lambda}\, h'$ for h' fixed across all schemes so that each scheme has the density ch'^{-3}. Wave speed errors across different schemes can then be compared as a function of $\boldsymbol{\xi}_{h'} = \boldsymbol{\xi} h'$. The computational density can also be written as $(\lambda^2/c^2)k^{-3}$ and this can be normalised to $(1/c^2)k'^{-3}$ by setting $k = \sqrt[3]{\lambda^2}k'$ for some k' fixed. Wave speed errors can then be compared as a function of $\omega_{k'} = \omega k'$. The densities of specific operations (additions, multiplications, memory reads) are obtained by multiplying the computational density by the number of specific operations carried out at each point-wise update. In most cases, for an N-point stencil using M shells of points, the number of multiplies is $M+1$, the number of additions is N, and the number of memory reads is $N+1$, at each point-wise update. Specific operations will not be considered because computation times depend on the specific computational hardware on which they are carried out. The computational density gives a rough idea of how the schemes should compare in practice, but exploring all the possible hardware implementations and specific operations is out of the scope of this study.

2.8. Simulation

A small simulation using the FD schemes in Fig. 2 is presented, as a motivating example, to demonstrate the effect of numerical dispersion on propagating waves in the FD schemes. These schemes were used to simulate Eq. (1) on a 1.41 m×1.41 m domain with c = 344 m/s. A spatial Gaussian with variance 0.007 was set as the initial condition with zero velocity and fixed boundaries (phase-inverting). The IWB scheme used F_s = 44.1 kHz. The grid spacings in the other scheme were adjusted such that all three had the same computational densities (each scheme has roughly 7.5×10^8 updates per square metre per second). Snapshots in time are shown in Fig. 3. The "exact" solution is seen in Fig. 4, which was obtained using a fourth-order accurate scheme (presented in the next section) with the grid spacing reduced by a factor of four (64x increase in computational density) so that numerical dispersion was negligible. The effect of the direction- and frequency-dependent wave speed error in Fig. 3 can be seen in the wakes of the propagating wave fronts; the directions of propagation in which the wave fronts stay sharp correspond to the directional dispersion seen in Fig. 2.

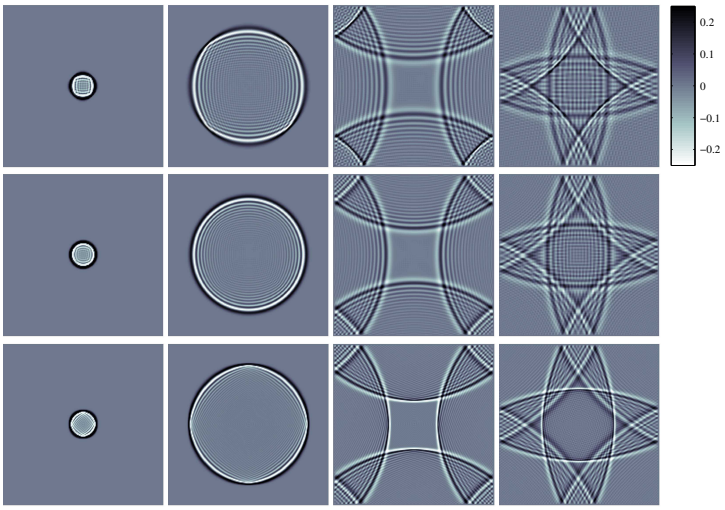

Figure 3: *Snapshots from simulation.* $\hat{u}(t, \boldsymbol{x})$ *at 0.03 ms, 1.5 ms, 3.5 ms, and 5 ms in five-point scheme (top), nine-point isotropic scheme (middle), and nine-point IWB scheme (bottom).*

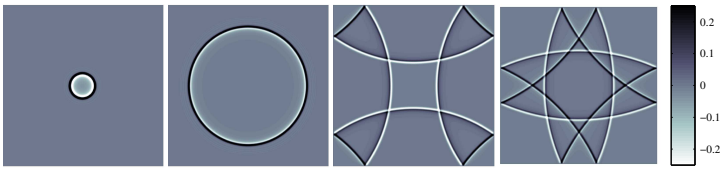

Figure 4: *Snapshots of "exact" solution* $\hat{u}(t, \boldsymbol{x})$ *at 0.03 ms, 1.5 ms, 3.5 ms, and 5 ms.*

3. FOURTH-ORDER SCHEMES

3.1. Fourth-order Accuracy

The d'Alembertian can be approximated to fourth-order accuracy in space and time by employing the modified equation method [9, 15]. Begin with the Taylor expansion of $\delta_\square \hat{u}$ in terms of h and k,

subject to the consistency constraint (7):

$$\delta_{\Box}\hat{u} = \Box\hat{u} + \frac{k^2\partial_t^4}{12}\hat{u} - \frac{c^2h^2}{60}((5\alpha_1 + 5\alpha_2 + 20\alpha_3 + 17\alpha_4 + 20\alpha_5)(\partial_x^4 + \partial_y^4) + (30\alpha_2 + 48\alpha_4 + 120\alpha_5)\partial_x^2\partial_y^2)\hat{u} + O(h^4) + O(k^4)\,. \quad (16)$$

The truncation error is currently $O(h^2) + O(k^2)$, and the scheme is thus second-order accurate. The parameters in $\boldsymbol{\alpha}$ are to be constrained such that the biharmonic operator Δ^2 appears in the error. This makes the error isotropic (directionally independent) up to fourth-order terms. The condition for fourth-order isotropy is:

$$5\alpha_1 - 10\alpha_2 + 20\alpha_3 - 7\alpha_4 - 40\alpha_5 = 0\,. \quad (17)$$

Applying this condition results in the following:

$$\delta_{\Box}\hat{u} = \Box\hat{u} + \frac{1}{12}(k^2\partial_t^4 - c^2h^2F_1(\boldsymbol{\alpha})\Delta^2)\hat{u} + O(h^4) + O(k^4)\,, \quad (18)$$

where $F_1(\boldsymbol{\alpha})$ is an affine function of $\boldsymbol{\alpha}$ subject to the two constraints (7) and (17). With c constant, the Courant number $\lambda = ck/h$, $\lambda > 0$, is set to a constant such that:

$$F_1(\boldsymbol{\alpha}) = \lambda^2\,, \quad (19)$$

which gives:

$$\delta_{\Box}\hat{u} = \Box\hat{u} + \frac{k^2}{12}(\partial_t^2 - c^2\Delta)(\partial_t^2 + c^2\Delta)\hat{u} + O(k^4)\,, \quad (20)$$

$$\delta_{\Box}\hat{u} = (1 + O(k^2))\Box\hat{u} + O(k^4)\,. \quad (21)$$

Using Eq. (8) results in a fourth-order accurate approximation to the d'Alembertian:

$$\delta_{\Box}\hat{u} = \Box\hat{u} + O(k^4)\,. \quad (22)$$

Choices of λ and $\boldsymbol{\alpha}$ satisfying (7), (17), and (19) result in a FD scheme with a truncation error that is $O(k^4)$. According to the Lax-Richtmyer theorem [21], the FD approximation $\hat{u}(t, \boldsymbol{x})$ will converge to the solution $u(t, \boldsymbol{x})$ with $O(k^4)$ as $k \to 0$ for fixed λ chosen such the scheme is numerically stable.

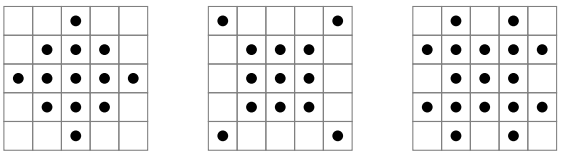

(a) *13-point #1* (b) *13-point #2* (c) *17-point #1*

Figure 5: *Points on square grid used for discrete Laplacians.*

3.2. Fourth-order Accurate Anisotropic Schemes

Special cases of the 25-point family will now be investigated. Within this family there eight possible ways to use the sets $\Omega_j \in \Upsilon$ to choose a 13-point stencil, seven ways to choose a 17-point stencil, and four ways to choose a 21-points stencil. Only certain stencils are featured, specifically those that include the sets Ω_1 and Ω_2. The stencils that do not have both Ω_1 and Ω_2 were found to have poor numerical dispersion not worth reporting, or they did not allow stable fourth-order schemes.

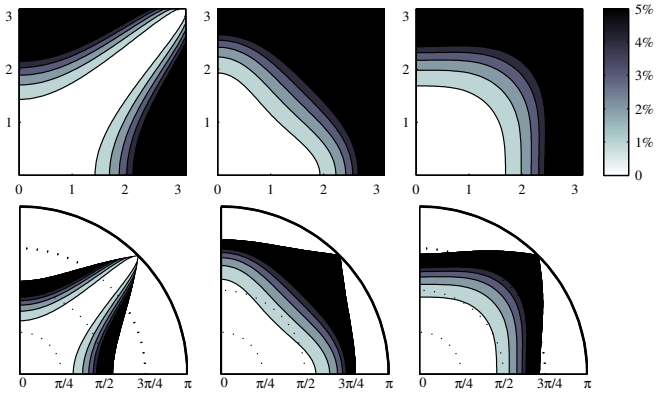

(a) *13-point #1* (b) *13-point #2* (c) *17-point #1*

Figure 6: *Optimal anisotropic fourth-order accurate schemes, relative wave speed error* $(|1 - \hat{\nu}|)$ *as a function of* $\boldsymbol{\xi}_h$ *(top row) and as a function of* ω_k *and* θ *(bottom row). Contours denote 1% deviations in the error. Any error beyond 5% is coloured in black.*

Two 13-point schemes, with $\alpha_4 = \alpha_5 = 0$ and $\alpha_3 = \alpha_4 = 0$ respectively, and a 17-point scheme with $\alpha_3 = \alpha_5 = 0$ [15] will be investigated first. The spatial points used in these schemes are shown in Figs. 5a-5c. These schemes have four free parameters (λ and three in $\boldsymbol{\alpha}$), but have four constraints: consistency (7), isotropy (17), accuracy (19), and stability (13). There is an upper bound on λ for stability so there is still a free parameter, in a sense. However, for audio purposes it is generally best to set $\lambda = \lambda_{\max,\boldsymbol{\alpha}}$ to minimise numerical dispersion and maximise cutoff frequencies [13, 15]. This might be called the "audio constraint". The fourth-order scheme for each stencil that satisfies all of these constraints (if it exists) will be called the "optimal scheme". Since the leading error term in these schemes is not isotropic, they will further be called the "anisotropic" optimal fourth-order schemes. The parameters of the optimal schemes are listed in Table 1 and their wave speed errors are plotted in Figs. 6a-6c. In Table 1 only α_1 is given for brevity; the rest of $\alpha_i \neq 0$ can be determined from (7) and (17).

In general, the numerical dispersion around DC ($|\boldsymbol{\xi}| = 0$ or

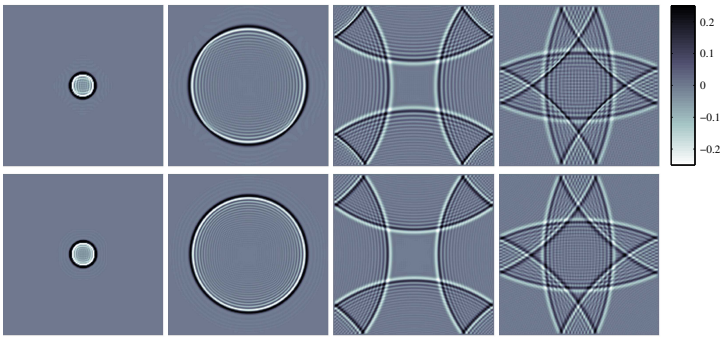

Figure 7: *Snapshots from simulation.* $\hat{u}(t, \boldsymbol{x})$ *at 0.03 ms, 1.5 ms, 3.5 ms, and 5 ms for 13-point #1 scheme (top) and 17-point #1 scheme (bottom).*

Table 1: *Parameters for optimal fourth-order schemes*

Scheme	α_1	λ^2	λ (approx.)
13-point #1	1	$1/2$	0.707
13-point #2	$\sqrt{1/3}$	$\sqrt{3}/2$	0.930
17-point #1	$11/16$	$3/4$	0.866
17-point #2	$(8+\sqrt{14})/15$	$3(8-\sqrt{14})/20$	0.799
21-point #1	$(22+5\sqrt{11})/60$	$3(6-\sqrt{11})/10$	0.897
21-point #2	$\sqrt{181}/20$	$3(16-\sqrt{181})/10$	0.874

$\omega = 0$) is reduced in the fourth-order schemes, as seen in Figs. 6a-6c. The relative wave speed along the worst-case direction for each scheme is plotted in Fig. 10, after normalising for computational densities. Fig. 10 shows that the fourth-order schemes maintain a flatter wave speed error in lower frequencies than the second-order schemes; this is a consequence of better agreement with the wave equation.

The optimal 13-point #1 and the 17-point #1 schemes were used to repeat the previous simulation (with 7.5×10^8 updates per square metre per second). Snapshots in time can be seen in Fig. 7. In general, the wave fronts in Fig. 7 are more sharp than the five-point scheme and the nine-point isotropic scheme. The wave fronts travelling in directions diagonal to the grid axes have less dispersion than the IWB scheme.

3.3. Fourth-order Accurate Isotropic Schemes

Three more schemes that use an extra shell of points and an extra free parameter are investigated next. These include a 17-point scheme with $\alpha_4 = 0$ and two 21-point schemes with $\alpha_5 = 0$ and $\alpha_3 = 0$ respectively. The stencils are shown in Figs. 8a-8c.

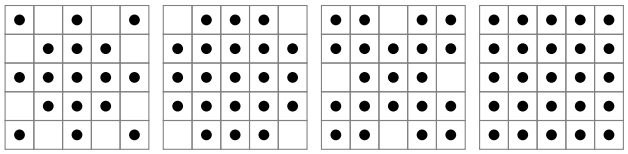

(a) *17-point #2* (b) *21-point #1* (c) *21-point #2* (d) *25-point*

Figure 8: *Points on square grid used for discrete Laplacians.*

With the extra free parameter another constraint can be employed to achieve isotropy up to the sixth-order terms in the error. Using a Taylor expansion, along with (7) and (23), this extra condition is found to be:

$$\alpha_1 - 4\alpha_2 + 16\alpha_3 - 7\alpha_4 - 64\alpha_5 = 0\,. \tag{23}$$

Now with (17) the Taylor expansion gives:

$$\delta_\square \hat{u} = \square\hat{u} + \frac{1}{12}(k^2\partial_t^4 - c^2h^2F_1(\boldsymbol{\alpha})\Delta^2)\hat{u} + \frac{1}{360}(k^4\partial_t^6 - c^2h^4F_2(\boldsymbol{\alpha})\Delta^3)\hat{u} + O(h^6) + O(k^6) \tag{24}$$

where $F_2(\boldsymbol{\alpha})$ is an affine function of $\boldsymbol{\alpha}$ subject to the three constraints (7), (23), and (17).

An additional constraint, $F_2(\boldsymbol{\alpha}) = \lambda^4$, could be added to achieve sixth-order accuracy [15], but it was found that none of the sixth-order accurate schemes within the 25-point family is stable. In fact, after employing the full 25-point stencil shown in Fig. 8d, the constraint for sixth-order accuracy leads to $\lambda = 1$, but von Neumann analysis revealed that $\lambda_{\max,\boldsymbol{\alpha}} \approx 0.99$. A stable sixth-order accurate scheme can be found by including the next (sixth) shell of points on the square grid: $\Omega_6 = \{3\hat{\boldsymbol{e}}_x, 3\hat{\boldsymbol{e}}_y\}$ [15, 22].

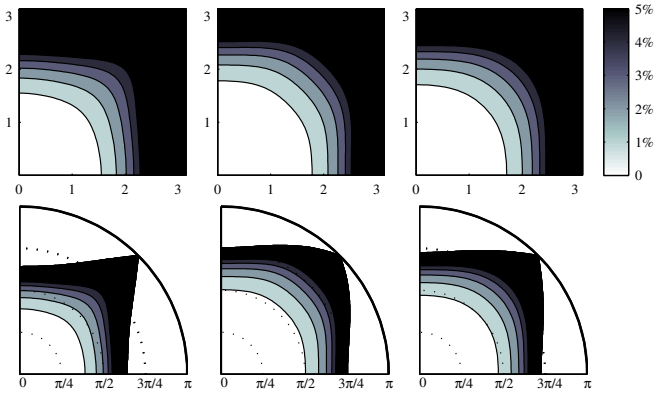

(a) *17-point #2* (b) *21-point #1* (c) *21-point #2*

Figure 9: *Optimal isotropic fourth-order accurate schemes, relative wave speed error* $(|1-\hat{\nu}|)$ *as a function of* $\boldsymbol{\xi}_h$ *(top row) and as a function of* ω_k *and* θ *(bottom row). Contours denote 1% deviations in the error. Any error beyond 5% is coloured in black.*

An extra constraint could also be employed for eighth-order isotropy with the 25-point stencil, however it was found that the 25-point fourth-order accurate, eight-order isotropic scheme is not stable, so fourth-order accuracy must be abandoned to include eight-order isotropy, leaving only second-order accuracy. An "optimal" fourth-order 25-point scheme cannot be identified without an extra constraint for the last free parameter, so 25-point schemes will only be investigated in the next section with optimisation.

The optimal isotropic 17- and 21-point fourth-order accurate schemes are then listed in Table 1 and their wave speed errors are displayed in Fig. 9. In Fig. 10, the relative wave speed for the worst-case direction in each scheme is plotted as a function of temporal frequencies after normalising for computational densities.

4. OPTIMISED SCHEMES

Optimisation can be conducted on the 13- to 25-point schemes in order to minimise wave speed error over a wider range of wavenumbers. In [15], a weighted mean square error was defined over a range of wavenumbers and minimised using optimisation. Another strategy is to maximise the "critical wavenumber" under which the absolute wave speed error is less than some threshold in every direction, after normalising for computational densities [13]. More formally, for some wave speed error threshold $0 < \varepsilon < 1$ the goal is to find $\boldsymbol{\alpha}$ such that the critical wavenumber, $|\boldsymbol{\xi}^*_{h'}|$, is maximised:

$$\arg\max_{\boldsymbol{\alpha}} |\boldsymbol{\xi}^*_{h'}| : |1-\hat{\nu}(\boldsymbol{\xi}_{h'})| \le \varepsilon\,, \quad \forall \boldsymbol{\xi}_{h'} : |\boldsymbol{\xi}_{h'}| \le |\boldsymbol{\xi}^*_{h'}|\,. \tag{25}$$

As in [13, 15], it is assumed that $\lambda = \lambda_{\max,\boldsymbol{\alpha}}$ (determined numerically). A one percent error criterion will be used ($\varepsilon = 0.01$), and the value $|\boldsymbol{\xi}^*_{h'}|$ from (25) will be known as the "1% bandwidth" (1% BW). The gain in the 1% BW obtained over the optimal counterpart will be known as the "bandwidth extension" (BWE).

Optimisation was performed over the entire range of free parameters in $\boldsymbol{\alpha}$, but $\boldsymbol{\alpha}$ was constrained for consistency (7) and such

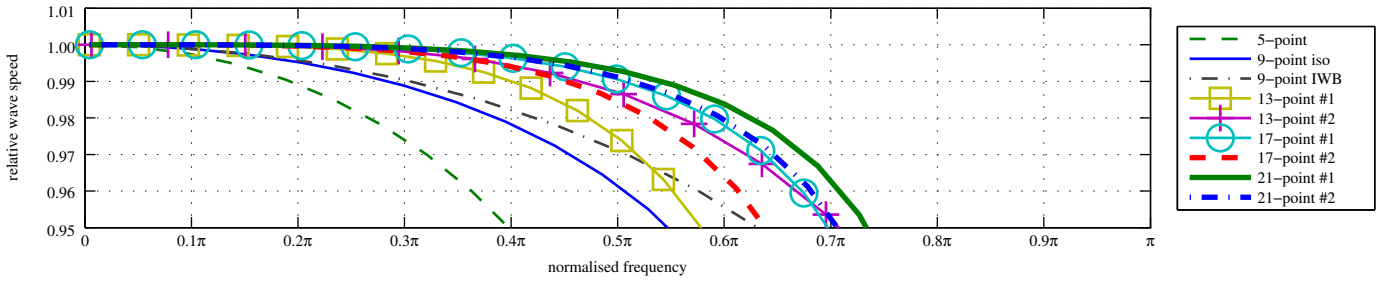

Figure 10: *Relative wave speeds of optimal fourth-order schemes, and second-order schemes, as a function of normalised frequency $\omega_{k'}$ (also normalised for computational density), along respective worst-case directions.*

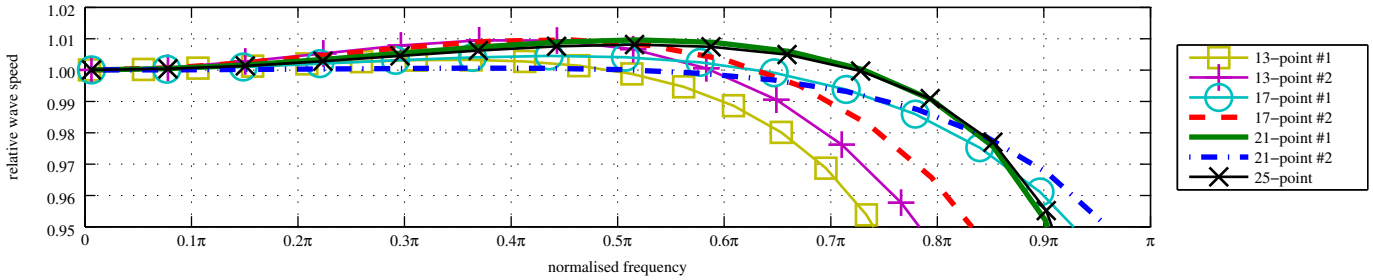

Figure 11: *Relative wave speeds of optimised fourth-order schemes as a function of normalised frequency $\omega_{k'}$ (also normalised for computational density), along respective worst-case directions.*

that $\mathcal{D}_{\boldsymbol{\Delta},\boldsymbol{\alpha},\Upsilon}$ remained non-positive (checked numerically). A combination of gradient descent and the Nelder-Mead simplex method was used. As the search space is large and exhibits complex behaviour, mainly due to the non-linearity in $\lambda_{\max,\boldsymbol{\alpha}}$, the optimisation of each scheme began from its optimal parameters with some small random perturbations. The schemes found through optimisation will be referred to as "optimised schemes", as opposed to the "optimal schemes" given previously.

The parameters of the optimised schemes are provided in Table 2, along with the five-point and nine-point schemes, for reference. The optimised parameters $\boldsymbol{\alpha}$ were rounded to three decimal places, then $\lambda \approx \lambda_{\max,\boldsymbol{\alpha}}$ was determined and truncated (rounding could violate (13)). Also found in Table 2 are the 1% BW, the BWE, and $\|\Delta\boldsymbol{\alpha}\|$, which represents the Euclidean norm of the vector $\Delta\boldsymbol{\alpha}$ that takes the optimal scheme to the optimised scheme in the $\boldsymbol{\alpha}$ parameter space ($\mathbb{R}^5$). These values are rounded to three decimal places. The second last column shows the *relative computational efficiency* (RCE) [13], which represents the factor by which the computational density can decrease in a scheme to meet the 1% BW of some reference scheme (in this case, the five-point scheme [13]). The RCEs were calculated before 1% BW values were rounded. The last column in Table 2 shows the change in the RCEs obtained over the optimal counterparts. Note that the RCE for a given ε is independent of the frequency [13] The RCE has been calculated via $\hat{\nu}(\omega_k(|\boldsymbol{\xi}_h|,\theta),\theta)$ [13], but it is equally (and more easily) calculated using $\hat{\nu}(\boldsymbol{\xi}_h)$, since, ultimately, the measure is independent of the frequency.

It can be seen that in every optimised scheme there is a significant BWE and change in the RCE (the ΔRCE) over the optimal counterpart. It is interesting to note that often the optimised scheme is relatively far from the optimal counterpart in the $\boldsymbol{\alpha}$ parameter space, as seen by the values of $\|\Delta\boldsymbol{\alpha}\|$. The wave speed errors are plotted in Fig. 13. In Fig. 11, the relative wave speed for the worst-case direction in each optimised scheme is plotted as a function of temporal frequencies after normalising for computational densities. An improvement over the optimal counterparts is clear from a comparison of Figs. 6 and 9 to Figs. 13, and from a comparison of Fig. 10 to Fig. 11. The RCEs of the optimised schemes are also significantly higher than nine-point schemes. They are also higher than a fourth-order accurate implicit nine-point scheme presented in [13], which had a RCE of 12.3, and some are higher than another optimised implicit nine-point scheme, which had a RCE of 41.9 [13].

The simulations presented previously were repeated for some of the optimised schemes, presented in Fig. 12. The approximated solutions in Fig. 12 maintain coherent wave fronts, moreso than the optimal fourth-order schemes. It is interesting to note that the relative wave speed is greater than unity for mid-range frequencies (also apparent from Fig. 11), so the wave fronts in the approximated solutions are a bit more advanced than in the exact solution.

A few details are worth noting about the optimised schemes. First, from the data in Table 2 it seems that adding the set Ω_5 does not effectively increase the 1% BW over the first 17-point scheme (to go to the second 21-point scheme), and likewise for the first 21-point scheme (to go to the 25-point scheme). In fact, the $\boldsymbol{\alpha}$ parameters do not change significantly and α_5 remains close to zero, although the optimisation might not have found a better scheme, if one exists. The schemes presented here are not guaranteed to pertain to global maxima, since the search space is not well studied nor understood yet.

Second, the criterion that was used to disregard certain stencils in Section 3 is by no means a general rule of thumb. See [15] for

Table 2: *Parameters for optimised schemes*

Scheme	α_1	α_2	α_3	α_4	α_5	λ	1% BW	BWE	$\|\Delta\boldsymbol{\alpha}\|$	RCE	ΔRCE
5-point	1.000	-	-	-	-	0.707	0.194π	-	-	1.00	-
9-point iso.	$0.66\bar{6}$	$0.33\bar{3}$	-	-	-	0.866	0.288π	-	-	3.24	-
9-point IWB	0.500	0.500	-	-	-	1.000	0.309π	-	-	4.00	-
13-point #1	0.948	0.298	-0.246	-	-	0.726	0.605π	0.199π	0.141	30.1	21.1
13-point #2	0.586	0.509	-	-	-0.095	0.923	0.659π	0.186π	0.043	38.8	24.5
17-point #1	0.660	0.494	-	-0.154	-	0.891	0.756π	0.245π	0.082	58.9	40.6
17-point #2	0.493	0.492	0.102	-	-0.087	1.005	0.707π	0.250π	0.380	48.1	35.1
21-point #1	0.591	0.532	0.077	-0.200	-	0.931	0.805π	0.258π	0.116	71.0	48.8
21-point #2	0.661	0.498	-	-0.187	0.028	0.894	0.763π	0.243π	0.122	60.3	41.2
25-point	0.601	0.532	0.067	-0.209	-0.009	0.925	0.806π	-	-	71.2	-

some schemes with stencils that do not include Ω_2 yet still have good dispersion and achieve sixth-order accuracy. Optimisation may reveal interesting schemes using the stencils that were left out.

Finally, and most importantly, the optimised schemes presented here do not explicitly satisfy fourth-order accuracy conditions, so they are only second-order accurate. Higher-order accuracy, in the traditional sense, is not necessary to effectively minimise numerical dispersion over a wide range of wavenumbers. However, stencils that lead to higher-order accuracy should also lead to interesting schemes through optimisation (this was also found in [13] for some nine-point implicit schemes). A spectral-like accuracy, such as the one used here [13] and those used in other studies [15, 23] is probably more appropriate for audio applications.

5. CONCLUSIONS

Fourth-order accurate explicit FD schemes for the 2-D wave equation employing special cases of a 25-point stencil on a square grid have been presented. Optimisation was performed in order to minimise wave speed error over a wide range of frequencies while taking into account computational densities. New FD schemes have been identified that offer better computational efficiency than 9-point schemes on the square lattice in terms of minimising one percent wave speed error up to some critical frequency.

Future work will focus on conducting perceptual tests that establish critical perceptual thresholds for wave speed error, in order to identify the most suitable FD scheme for audio applications (some preliminary tests have been conducted [24]). Another major area for future work will be to develop boundary conditions, beyond the simple fixed type, that can be coupled to these schemes and similar 3-D schemes [23] so that they may be used for room acoustics simulations.

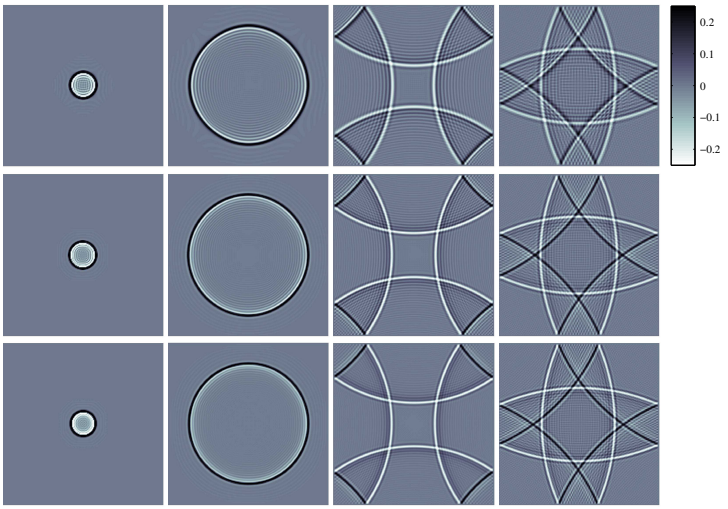

Figure 12: *Snapshots from simulation. $\hat{u}(t, \boldsymbol{x})$ at 0.03 ms, 1.5 ms, 3.5 ms, and 5 ms for optimised 13-point #1 scheme (top), 17-point #1 scheme (middle), and 21-point #1 scheme (bottom).*

6. REFERENCES

[1] R. Courant, K. Friedrichs, and H. Lewy, "Über die partiellen differenzengleichungen der mathematischen physik," *Mathematische Annalen*, vol. 100, no. 1, pp. 32–74, 1928.

[2] R. M. Alford, K. R. Kelly, and D. M. Boore, "Accuracy of finite-difference modeling of the acoustic wave equation," *Geophysics*, vol. 39, no. 6, pp. 834–842, 1974.

[3] S. A. van Duyne and J. O. Smith III, "Physical modeling with the 2-D digital waveguide mesh," in *Proc. Int. Computer Music Conf. (ICMC)*, Tokyo, Japan, 1993.

[4] D. T. Murphy and D. M. Howard, "Digital waveguide mesh topologies in room acoustics modelling," in *Proc. Digital Audio Effects (DAFx)*, Verona, Italy, 2000.

[5] S. Bilbao, *Numerical sound synthesis: finite difference schemes and simulation in musical acoustics*, Wiley, 2009.

[6] L. N. Trefethen, "Group velocity in finite difference schemes," *SIAM review*, vol. 24, no. 2, pp. 113–136, 1982.

[7] L. Savioja, "Real-time 3D finite-difference time-domain simulation of low-and mid-frequency room acoustics," in *Proc. Digital Audio Effects (DAFx)*, Graz, Austria, 2010, vol. 1, p. 75.

[8] C. J. Webb and A. Gray, "Large-scale virtual acoustics simulation at audio rates using three dimensional finite difference time domain and multiple GPUs," in *Proc. Int. Cong. Acoustics (ICA)*, Montréal, Canada, 2013.

[9] G. Cohen, "A class of schemes, fourth order in time and space, for the 2-D wave equation," in *Proceedings of the, Sixth IMACS International Symposium on Computer Methods for Partial Differential Equations, Bethlehem, USA*, 1987.

[10] L. Savioja and V. Välimäki, "Improved discrete-time modeling of multi-dimensional wave propagation using the interpolated digital waveguide mesh," in *Proc. IEEE ICASSP*, 1997, vol. 1, pp. 459–462.

[11] S. Bilbao, *Wave and scattering methods for the numerical integration of partial differential equations*, Ph.D. thesis, Stanford University, 2001.

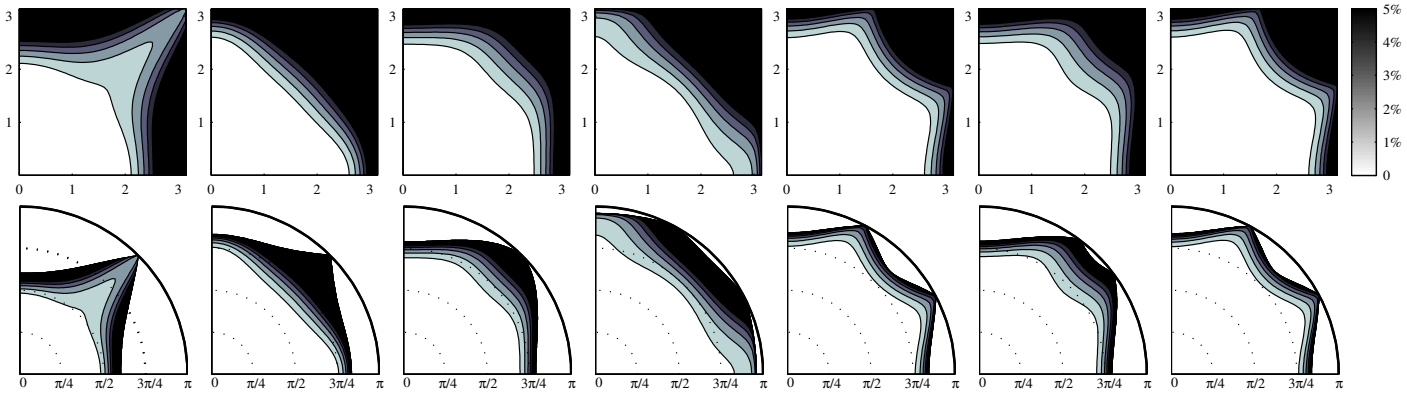

(a) *13-point #1* (b) *13-point #2* (c) *17-point #1* (d) *17-point #2* (e) *21-point #1* (f) *21-point #2* (g) *25-point*

Figure 13: *Optimised schemes, relative wave speed error* $(|1-\hat{\nu}|)$ *as a function of* $\boldsymbol{\xi}_h$ *(top row) and as a function* ω_k *and* θ *(bottom row). Contours denote 1% deviations in the error. Any error beyond 5% is coloured in black.*

[12] S. Bilbao, "Parameterized families of finite difference schemes for the wave equation," *Numerical Methods for Partial Differential Equations*, vol. 20, no. 3, pp. 463–480, 2004.

[13] M. van Walstijn and K. Kowalczyk, "On the numerical solution of the 2D wave equation with compact FDTD schemes," in *Proc. Digital Audio Effects (DAFx)*, Espoo, Finland, 2008, pp. 205–212.

[14] K. Kowalczyk and M. van Walstijn, "Room acoustics simulation using 3-D compact explicit FDTD schemes," *IEEE Trans. Audio, Speech, and Language Processing*, vol. 19, no. 1, pp. 34–46, 2011.

[15] S. Bilbao and B. Hamilton, "Construction and optimization techniques for high order schemes for the two-dimensional wave equation," in *Proc. Int. Cong. Acoustics (ICA)*, Montréal, Canada, 2013.

[16] G. Fairweather and A.R. Mitchell, "A high accuracy alternating direction method for the wave equation," *IMA J. Applied Mathematics*, vol. 1, no. 4, pp. 309–316, 1965.

[17] S. Bilbao and C. J. Webb, "Timpani drum synthesis in 3D on GPGPUs," in *Proc. Digital Audio Effects (DAFx)*, York, UK, 2012.

[18] S. K. Lele, "Compact finite difference schemes with spectral-like resolution," *J. Computational Physics*, vol. 103, no. 1, pp. 16–42, 1992.

[19] P. M. Morse and K. U. Ingard, *Theoretical acoustics*, Princeton University Press, 1968.

[20] J. G. Charney, R. Fjörtoft, and J. von Neumann, "Numerical integration of the barotropic vorticity equation," *Tellus*, vol. 2, no. 4, pp. 237–254, 1950.

[21] J. Strikwerda, *Finite difference schemes and partial differential equations*, Society for Industrial Mathematics, 2004.

[22] G. Cohen, *Higher-order numerical methods for transient wave equations*, Springer Verlag, 2002.

[23] S. Bilbao, "Optimized FDTD schemes for 3-D acoustic wave propagation," *IEEE Trans. Audio, Speech, and Language Processing*, vol. 20, no. 5, pp. 1658–1663, 2012.

[24] A. Southern, D. T. Murphy, T. Lokki, and L. Savioja, "The perceptual effects of dispersion error on room acoustic model auralization," in *Proc. Forum Acusticum, Aalborg, Denmark*, 2011, pp. 1553–1558.